Frequency Selective Surface Coded Retroreflectors for Chipless Indoor Localization Tag Landmarks

Alejandro Jiménez-Sáez, Martin Schüßler, Mohammed El-Absi, Ali Alhaj Abbas, Klaus Solbach, Thomas Kaiser, and Rolf Jakoby

***Abstract*—This letter presents the integration of frequency selective surfaces (FSSs) with retroreflectors for the realization of chipless wireless indoor localization tag landmarks. As an example, the high radar cross section (RCS) of a trihedral corner reflector is signed with an FSS-based stopband filter, so that the backscattered power from several corner reflectors can be distinguished by a mobile reader according to the frequency response of the FSS. Measurement results with a $3 \times 3 \times 3\,\text{cm}^3$ trihedral corner reflector and a stopband FSS in a Rogers RT/Duroid 5880 high-frequency laminate at 90 GHz shows an RCS above -25 dBsqm for 90° coverage in the TM plane. Due to the high RCS, measurements at distances up to 4 m with a standard 25 dBi gain horn antenna and a vector network analyzer as a reader are shown. These preliminary results show the potential of the concept for applications such as indoor localization with sub-mm accuracy, where high bandwidths, but only a low number of bits, are needed for the identification of the tag landmarks.**

***Index Terms*—Frequency selective surfaces, indoor localization, chipless radio-frequency identification (RFID), radar cross section (RCS).**

I. Introduction

FOR a performance increase in the automation and self-monitoring of industrial processes, improvements in the accuracy of indoor localization systems are needed. In self-localization systems, a mobile robot moving in an indoor environment can determine its position. Nowadays, the main factors limiting the spread of these systems in indoor environments are the cost of infrastructure, the localization accuracy, and reliability as well as the availability of compact, low cost, and energy-efficient readers.

State of the art indoor localization systems usually operate in the ISM bands below 10 GHz. This is mainly due to widespread technologies such as Wi-Fi, Bluetooth, and Zigbee, which allow the deployment of indoor localization systems at a reduced cost. However, the low available absolute bandwidth results in a low time resolution and therefore a limited localization accuracy. This accuracy decreases due to multipath effects, which affect the reliability of the system. Predictions at higher frequencies on the accuracy of 5G-based indoor localization methods show accuracies of several decimeters [1]. The advantages of designing localization systems in the millimeter-wave frequency range (30–300 GHz) are higher antenna gains and larger absolute bandwidths. Higher gains reduce the effect of multipath fading, while larger bandwidths increase the temporal resolution, allowing for a better localization accuracy and increased detection of multipath components.

For a successful self-localization system, an identification of each tag landmark is necessary. In the case of chipless radio-frequency identification (RFID) tags, the information is usually encoded in the frequency domain response of each tag. Other chipless alternatives include time-domain [2], phase [3], [4], and hybrid coding techniques [5]. An advantage of chipless RFID tags is their potential operation at high temperatures $T > 125\,^{\circ}\text{C}$, where the use of silicon components becomes increasingly difficult. Recently, the suitability of dielectric resonators for the realization of chipless RFID tag landmarks in the millimeter-wave frequency range has been studied for the component [6], [7], and system [8] levels. However, as the frequency increases, the geometrical size of the resonators decreases and with it the radar cross section (RCS). This effect results in low readout ranges below half a meter at 90 GHz in [6]. Components such as a dielectric lens increase the RCS by 24.4 dB in [7] at the expense of an increased design and manufacturing complexity.

While corner reflectors are widely used in long-range applications such as synthetic aperture radars [9], [10], the flatness of their frequency response limits their suitability for indoor localization due to the lack of identification. If a frequency selective surface (FSS) is integrated with a retroreflector, the response of the tag landmark becomes frequency selective and can be identified. At the same time, the high RCS and high operation frequencies in W-band allow for high-range resolution and corner reflector dimensions in the range of several centimeters. Some ideas for the realization of frequency selective retroreflectors are shown in [11] and [12] for dihedral and trihedral retroreflectors at 10 GHz and in [13] for spherical retroreflectors from 100 to 350 GHz.

In this letter, the integration of FSSs with trihedral corner reflectors for the coding of its frequency response in W-band is presented. Measurements are shown to demonstrate its potential for the differentiation of several targets in an indoor environment. Besides, the potential of this technology for accurate and reliable indoor positioning systems is discussed.

Manuscript received January 21, 2020; accepted February 14, 2020. Date of publication March 23, 2020; date of current version May 5, 2020. This work was supported by the Deutsche Forschungsgemeinschaft (DFG, German Research Foundation) under Project-ID 287022738 TRR 196, Projects C09 and S04. *(Corresponding author: Alejandro Jiménez-Sáez.)*

Alejandro Jiménez-Sáez, Martin Schüßler, and Rolf Jakoby are with the Institute of Microwave Engineering and Photonics, Technische Universität Darmstadt, 64289 Darmstadt, Germany (e-mail: aljimse@gmail.com; schuessler@imp.tu-darmstadt.de; jakoby@imp.tu-darmstadt.de).

Mohammed El-Absi, Ali Alhaj Abbas, Klaus Solbach, and Thomas Kaiser are with the Institute of Digital Signal Processing, University of Duisburg-Essen, 47057 Duisburg, Germany (e-mail: mohammed.el-absi@uni-due.de; ali.alhaj-abbas@uni-due.de; klaus.solbach@uni-due.de; thomas.kaiser@uni-due.de).

Digital Object Identifier 10.1109/LAWP.2020.2975143

This work is licensed under a Creative Commons Attribution 4.0 License. For more information, see https://creativecommons.org/licenses/by/4.0/

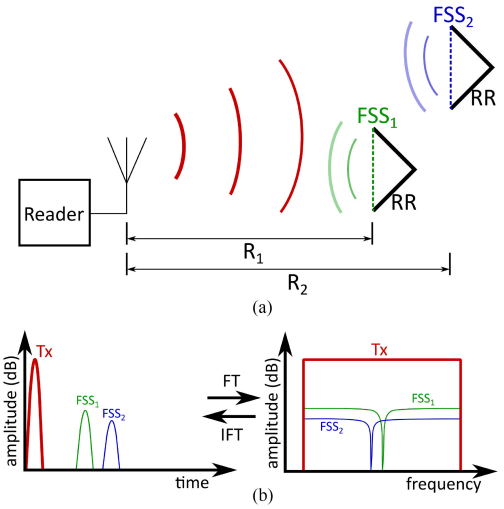

Fig. 1. (a) Block diagram of the system. (b) Transmitted and received signals by the reader in frequency and time domain. RR: Retroreflector, FT: Fourier Transform, and IFT: Inverse Fourier Transform.

II. Tag Concept

Fig. 1 shows a system model. The reader is a monostatic radar, i.e., a single antenna acts as a transmitter and receiver. The reader might be a vector network analyzer (VNA) or a more cost and size effective frequency modulated continuous wave (FMCW) radar as in [14]. More information on the use of FMCW radars as VNA-like measurement devices can be found in [15]–[18]. The tag can be divided into two parts: the retroreflector, in form of a dihedral reflector, a trihedral reflector, or a dielectric sphere as in [13], and a coding part, in this case, an FSS, to encode the information in the backscattered signal.

To maximize the bandwidth of the backscattered signal and increase the achievable range resolution, an FSS with a stopband response is designed. The FSS is placed in front of the retroreflector so that the retroreflected wave necessarily propagates through the FSS. In its stopband region, the FSS reflects the incident wave as a metal plate, so that the specular reflection is not backscattered toward the monostatic reader as long as it is not perfectly aligned with the tag. In its passband region, the incident wave propagates through the FSS and reaches the corner reflector, which reflects it in the same direction. Therefore, high bandwidth and high RCS over a broad angle allow for a stable and precise ranging, while a robust identification of the tag independent of the signal absolute magnitude is possible, permitting the use of this concept for the self-localization of a mobile robot.

III. FSS Characterization

A crossed dipole unit cell is chosen to avoid a polarization-dependent response of the FSS and a Rogers RT/Duroid 5880 high-frequency laminate with relative permittivity $\epsilon_r = 2.2$ is used. The unit-cell dimensions are summarized in Table I. The periodically spaced crossed dipoles are etched on one side and the copper ground is removed from the other side. For the characterization of the FSS, a two-port measurement with two standard 25 dBi gain horn antennas and a 32×32 FSS between both ports is performed. During the measurement, the FSS is rotated with an electric turntable and rotations in both the transversal magnetic (TM-) and transversal electric (TE-) planes are achieved by a 90° rotation of both the transmit and receive antennas. The results can be seen in Fig. 2.

TABLE I
Unit Cell Dimensions

Parameter	Value (mm)
Metal thickness	0.035
Unit cell width	2.26
Substrate thickness	0.127
Dipole length	1.48
Dipole width	0.25

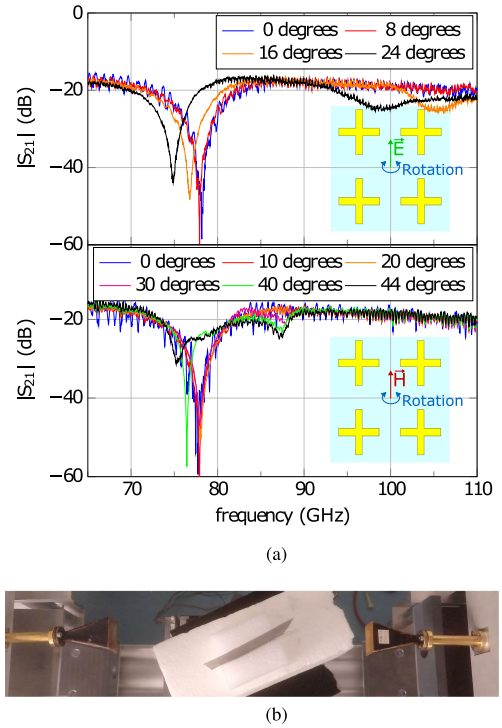

Fig. 2. (a) Transmission of the FSS over the angle for several angles and rotations in the TE-plane (top) and TM-plane (bottom). (b) FSS is placed between both ports and a 0° angle corresponds to normal incidence to the plane containing the FSS.

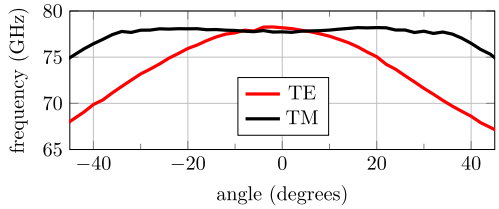

Fig. 3. Center frequency of the stopband over the incident angle.

An important outcome of this measurement is the fact that the stopband frequency of the FSS is stable for rotations in the TM-plane while it notably shifts against rotations in the TE-plane. The resonance frequency over the incident angle for both polarizations can be seen in Fig. 3. This occurs because the unit cells behave as dipoles, so their mutual coupling is stronger in the TE-plane. When the angle of the incident wave varies, each column of resonators is excited with a different phase and

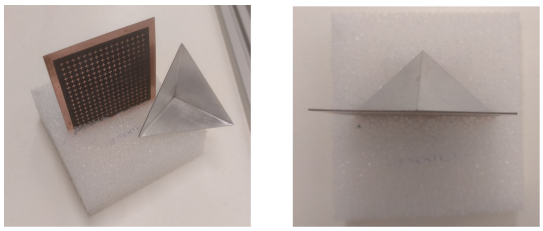

(a) (b)

Fig. 4. (a) Manufactured FSS (left) and trihedral corner reflector (right). (b) Top view of the tag, the corner reflector is positioned behind the FSS.

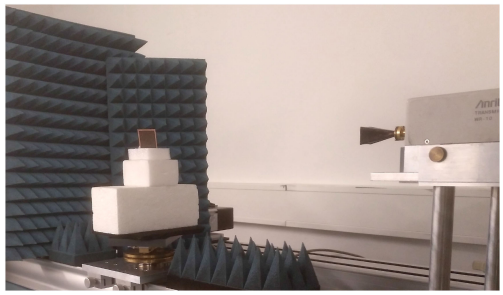

Fig. 5. Measurement setup for RCS measurements. A standard 25 dB gain horn antenna is used at the reader (right) and the tag is placed on a turntable and is held by foam (left). The distance between the reader and the tag is $d = 50$ cm.

the mutual coupling varies, shifting its resonance frequency. Since the mutual coupling is much weaker in the TM-plane, this frequency shift lower than 0.8 GHz $\approx 1\%$ for incident angles below $\pm 36^\circ$.

IV. Frequency Selective Retroreflective Tags

For these measurements, a $3 \times 3 \times 3$ cm^3 trihedral corner reflector of triangular cross section has been used. An FSS with 16×16 unit cells is placed in front of it as shown in Fig. 4.

The measurement setup for the characterization of the target in W-band is shown in Fig. 5. To calculate the RCS, a metallic sphere with a radius of 10 mm is used as a reference. The unknown RCS of a target σ_u can be calculated as

$$\sigma_u = \frac{|S_{11\_u}|^2}{|S_{11\_\text{ref}}|^2}\sigma_{\text{ref}} \tag{1}$$

where S_{11_u} and S_{11_ref} are the scattering parameters measured in the VNA and σ_{ref} is the RCS of a reference object. A metallic sphere with RCS $\sigma_{\text{ref}} = \pi r^2$ is used as reference. For the measurement of the RCS, a differential measurement with and without the tag is performed. All RCS measurements are taken at a constant distance of 50 cm.

The tag is placed on an electric turntable and the incident polarization for the TM and TE measurements is changed by a 90° rotation of the reader antenna. The measured frequency response for several angles is shown in Fig. 6. A notch in the response can be distinguished at the frequencies shown in Figs. 2 and 3. The RCS over the angle at 90 GHz can be seen in Fig. 7. Since the incident wave is specularly reflected at the resonance frequency of the FSS, such contribution is reflected toward the reader only for normal incidence. For this reason, the notch cannot be clearly distinguished at normal incidence.

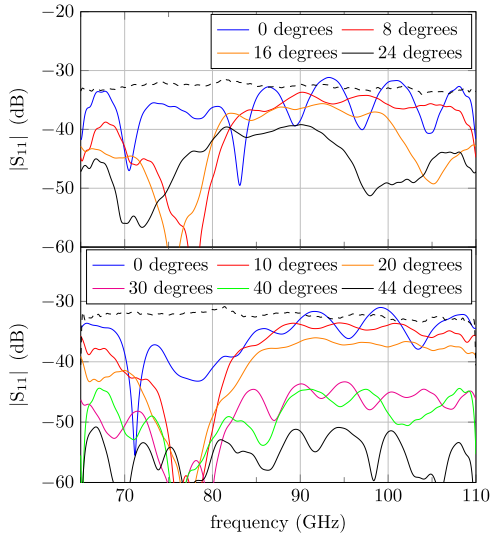

Fig. 6. Frequency response at different angles when the tag is rotated in the TE-plane (top) and TM-plane (bottom). The tag response is more stable when the tag is rotated in the TM-plane. The response of the corner reflector without an FSS at 0° incidence is shown in a black dashed line as a reference.

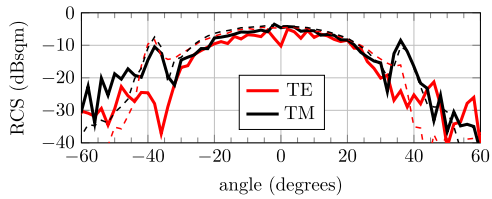

Fig. 7. RCS at 90 GHz over the incident angle for rotations in the TE and TM planes. The dashed lines represent the response of the trihedral corner reflector without an FSS.

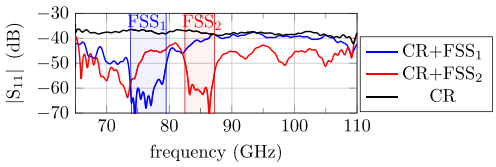

Fig. 8. Difference between two FSS coded and uncoded trihedral CRs.

Fig. 8 shows the measurement of two coded corner reflectors FSS_1 and FSS_2. The operation frequency of FSS_2 is shifted by placing a 700 μm thick fused silica slab in front of it. The tags are placed at a distance of 67 and 57 cm from the reader and the readout of both reflectors is performed from a single measurement by time gating the received signal.

The performance of the tag is analyzed at different distances in the laboratory with no absorbing materials nor differential measurement. Time gating is used to reduce clutter with a rectangular window that starts 1 ns before and ends 2 ns after the received pulse in the time domain signal in Fig. 9. The measured frequency response for distances from 1 to 4 m is shown in Fig. 9. As expected, the power decay at different distances decreases with the fourth power of the distance.

Fig. 10 depicts the error probability of ranging the proposed tag to its distance versus the signal-to-noise ratio (SNR) of the

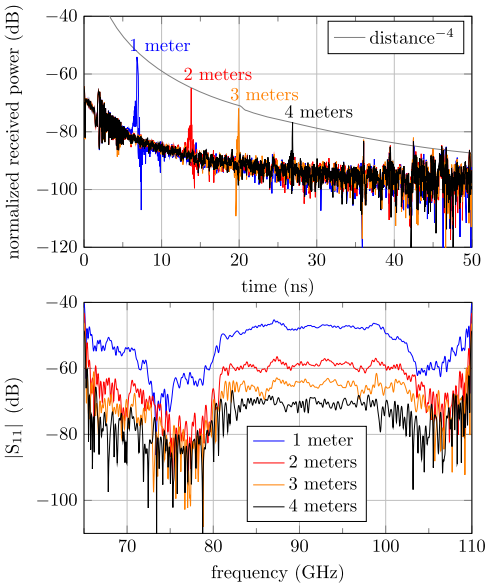

Fig. 9. (a) Time-domain response at distances from 1 to 4 m in a laboratory environment with line-of-sight and a TM incident angle equal to 12°. The reflected pulses by the tags can be easily distinguished from the clutter. Some late reflections due to other furniture and measurement equipment can be seen after 35 ns. (b) Time-gated frequency domain response.

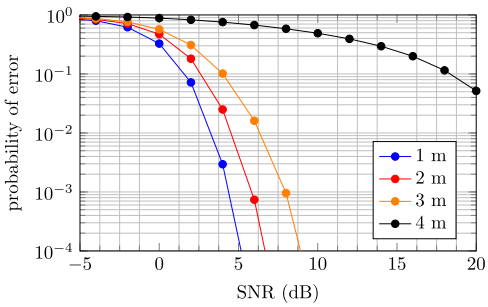

Fig. 10. Error probability of ranging by peak detection. The signals used for the simulation are shown in Fig. 9 and the first 5 ns are filtered out.

backscattered signal for the four distances shown in Fig. 9. For shorter distances, the required SNR for ranging the tag is lower. The probability of ranging error decreases with the increase of the SNR. The tag is efficiently detected even with low SNR up to 3 m. Detecting the tag located 4 m from the reader is still feasible, but a larger SNR is needed.

V. Discussion

One of the main issues of chipless wireless RFID tags, especially but not only at higher frequencies, is the low RCS of the passive tags. This low backscattered power results in low ranges and often needs a previously calibrated environment, limiting the number of applications where chipless wireless RFID tags can be used. In the case of indoor self-localization, an unknown environment needs to be assumed and ranges of several meters are desired. However, the number of bits might be kept low, since a smart positioning of tag landmarks and the continuity in the movement of the mobile robot in a room permit the reuse of identification codes in several locations.

TABLE II
RCS Comparison

	Result type	Freq. (GHz)	RCS (dBsqm)
Metallic sphere d = 20 mm	Analytical	-	-35.0
Cylindrical DR [8]	Sim. (Lossless)	105	-51.9
[8] with lens	Sim. (Lossless)	105	-26...-29
[19] DR in a photonic crystal	Measurement	90.4	-43.3
This paper	Measurement	90	-5...-30

The presented results demonstrate the possibility to alter the frequency response of trihedral corner reflectors and how large distances can be covered with compact corner reflectors. In Table II, these results are compared with other recently published results. Compared to single-resonator approaches, the RCS is incremented by 30 dB or a factor 1000 so that the range is more than five times larger. Notice that, by increasing the reader antenna gain by 6 dB, the range is theoretically doubled according to the radar equation.

However, the drawback of this method in comparison with the single resonator approach is the number of different retroreflectors that can be distinguished. Assuming a $\pm 45^\circ$ TM-plane coverage per corner reflector, a 4 GHz separation per tag is needed according to Fig. 3, resulting in a maximum number of 8 tags or 3 bits in the W-band (75–110 GHz). If the coverage is reduced to $\pm 36^\circ$, 1.1 GHz could be used per corner reflector, resulting in a maximum number of 32 tags or 5 bits in the whole W-band. This is a low amount of bits for the wide bandwidth being used and limits the applications where this technology could be used. Single [20] and multilayer [21] angularly stable FSSs at frequencies from 1 to 10 GHz can be found in the literature. Also, dual-band FSSs would allow for multiresonator coding techniques [22], [23] in a single retroreflector. The use of these angularly stable designs at 90 GHz is possible but would require a higher fabrication accuracy due to the 50 μm wide structures. Also, advanced modulation techniques may be appropriate, which use the frequency shift for the detection of the angle of arrival while being able to successfully identify several retroreflectors. Besides, different implementations or an accurate time gating should be able to avoid the different response at 0° incidence which origins from the superposition of the reflected pulses at the FSS and the corner reflector.

VI. Conclusion

These preliminary results show the potential of the integration of frequency-selective structures with retroreflectors for indoor localization. The high RCS and wide readout angles and simple structure make them suitable for low-loss durable RFID tag landmarks. Moreover, the wide RCS bandwidth allows for precise localization. Besides, the concept is easily scalable to higher frequencies, where the dimensions can be further reduced and the positioning accuracy increased. Current drawbacks are the response for normal incidence or the low number of bits that can be coded in a given bandwidth, for which further research is needed.

Acknowledgment

The authors would like to thank CST Studio Suite.

REFERENCES

[1] O. Kanhere and T. S. Rappaport, "Position locationing for millimeter wave systems," in *Proc. IEEE Global Commun. Conf.*, 2018, pp. 206–212.

[2] A. Ramos, A. Lazaro, D. Girbau, and R. Villarino, "Time-domain measurement of time-coded UWB chipless RFID tags," *Prog. Electromagn. Res.*, vol. 116, pp. 313–331, 2011.

[3] M. Schüßler, C. Mandel, M. Maasch, A. Giere, and R. Jakoby, "Phase modulation scheme for chipless RFID-and wireless sensor tags," in *Proc. Asia Pac. Microw. Conf.*, 2009, pp. 229–232.

[4] I. Balbin and N. C. Karmakar, "Phase-encoded chipless RFID transponder for large-scale low-cost applications," *IEEE Microw. Wireless Compon. Lett.*, vol. 19, no. 8, pp. 509–511, Aug. 2009.

[5] A. Jiménez-Sáez, M. Schüßler, M. Nickel, and R. Jakoby, "Hybrid time-frequency modulation scheme for chipless wireless identification and sensing," *IEEE Sensors J.*, vol. 18, no. 19, pp. 7850–7859, Oct. 2018.

[6] A. Jiménez-Szez, M. Schüßler, R. Jakoby, C. Krause, F. Meyer, and G. Vom Bögel, "Photonic crystal THz high-Q resonator for chipless wireless identification," in *Proc. 1st Int. Workshop Mobile Terahertz Syst.*, 2018, pp. 1–5.

[7] A. A. Abbas, M. El-Absi, A. Abuelhaija, K. Solbach, and T. Kaiser, "RCS enhancement of dielectric resonator tag using spherical lens," *Frequenz*, vol. 73, no. 5/6, pp. 161–170, 2019.

[8] M. El-Absi, A. A. Abbas, A. Abuelhaija, F. Zheng, K. Solbach, and T. Kaiser, "High-accuracy indoor localization based on chipless RFID systems at THz band," *IEEE Access*, vol. 6, pp. 54355–54368, 2018.

[9] A. Freeman, "SAR calibration: An overview," *IEEE Trans. Geosci. Remote Sens.*, vol. 30, no. 6, pp. 1107–1121, Nov. 1992.

[10] Y. Zhou, C. Li, L. Ma, M. Y. Yang, and Q. Liu, "Improved trihedral corner reflector for high-precision SAR calibration and validation," in *Proc. IEEE Geosci. Remote Sens. Symp.*, 2014, pp. 454–457.

[11] A. Lazaro, J. Lorenzo, R. Villarino, and D. Girbau, "Modulated corner reflector using frequency selective surfaces for FMCW radar applications," in *Proc. Eur. Microw. Conf.*, 2015, pp. 111–114.

[12] I. L. Morrow, K. Morrison, M. Finnis, and W. Whittow, "A low profile retrodirective frequency selective surface for radar earth observation," in *Proc. Loughborough Antennas Propag. Conf.*, 2015, pp. 1–4.

[13] R. J. Williams, A. J. Gatesman, T. M. Goyette, and R. H. Giles, "Radar cross section measurements of frequency selective terahertz retroreflectors," *Proc. SPIE*, vol. 9102, 2014, Art. no. 91020R.

[14] N. Pohl *et al.*, "Radar measurements with micrometer accuracy and nanometer stability using an ultra-wideband 80 GHz radar system," in *Proc. IEEE Top. Conf. Wireless Sensors Sensor Netw.*, 2013, pp. 31–33.

[15] A. G. Stove, "Linear FMCW radar techniques," *IEE Proc. F, Radar Signal Process.*, vol. 139, no. 5, pp. 343–350, 1992.

[16] T. Hauschild and R. Knochel, "Calibration of short range FMCW-radars with network analyzer calibration techniques," *IEEE MTT-S Int. Microw. Symp. Dig.*, 1998, vol. 2., pp. 969–972.

[17] J. Barowski, M. Zimmermanns, and I. Rolfes, "Millimeter-wave characterization of dielectric materials using calibrated FMCW transceivers," *IEEE Trans. Microw. Theory Techn.*, vol. 66, no. 8, pp. 3683–3689, Aug. 2018.

[18] J. Barowski *et al.*, "Design and evaluation of a passive frequency-coded reflector using W-band FMCW radar," in *Proc. German Microw. Conf.*, 2020, accepted for publication.

[19] A. Jiménez-Sáez, M. Schüßler, D. Pandel, N. Benson, and R. Jakoby, "3D printed 90 GHz frequency-coded chipless wireless RFID tag," in *Proc. IEEE MTT-S Int. Microw. Workshop Series Adv. Mater. Processes RF THz Appl.*, 2019, pp. 4–6.

[20] T. Hong, W. Xing, Q. Zhao, Y. Gu, and S. Gong, "Single-layer frequency selective surface with angular stability property," *IEEE Antennas Wireless Propag. Lett.*, vol. 17, no. 4, pp. 547–550, Apr. 2018.

[21] S. Azemi, K. Ghorbani, and W. Rowe, "Angularly stable frequency selective surface with miniaturized unit cell," *IEEE Microw. Wireless Compon. Lett.*, vol. 25, no. 7, pp. 454–456, Jul. 2015.

[22] C.-N. Chiu and W.-Y. Wang, "A dual-frequency miniaturized-element FSS with closely located resonances," *IEEE Antennas Wireless Propag. Lett.*, vol. 12, pp. 163–165, 2013.

[23] S. Ghosh and K. V. Srivastava, "An angularly stable dual-band FSS with closely spaced resonances using miniaturized unit cell," *IEEE Microw. Wireless Compon. Lett.*, vol. 27, no. 3, pp. 218–220, Mar. 2017.